Proceedings of ASME-IMECE 2004
International Mechanical Engineering Congress and Exposition
November 13-19, 2004, Anaheim, California, U.S.A.

IMECE2004-60210

THERMAL CONTROL UTILIZING AN ELECTROHYDRODYNAMIC CONDUCTION PUMP IN A TWO-PHASE LOOP WITH HIGH HEAT FLUX SOURCE

Seong-il Jeong

Research Associate,
National Research Council,
National Academies of Science
sjeong@mscmail.gsfc.nasa.gov

Jeffrey Didion

Thermal Technology Development,
NASA Goddard Space Flight Center,
Greenbelt, Maryland 20771, USA
Jeffrey.R.Didion@nasa.gov

ABSTRACT

The electric field applied in dielectric fluids causes an imbalance in the dissociation-recombination reaction generating free space charges. The generated charges are redistributed by the applied electric field resulting in the heterocharge layers in the vicinity of the electrodes. Proper design of the electrodes generates net axial flow motion pumping the fluid. The electrohydrodynamic (EHD) conduction pump is a new device that pumps dielectric fluids utilizing heterocharge layers formed by imposition of electrostatic fields. This paper evaluates the experimental performance of a two-phase breadboard thermal control loop consisting of an EHD conduction pump, condenser, pre-heater, high heat flux evaporator (HE), transport lines, and reservoir (accumulator). The generated pressure head and the maximum applicable heat flux are experimentally determined at various applied voltages and sink temperatures. Recovery from dryout condition by increasing the applied voltage to the pump is also demonstrated.

INTRODUCTION

The capillary pumping devices such as heat pipes, capillary pumped loops(CPLs) and loop heat pipes(LHPs) have been used for thermal control for many years. They are two-phase heat transfer devices that transfer heat with little temperature difference. The capillary force developed by the wick structure circulates the fluid. Therefore, the capillary pumping capacity is the primary limitation governing the operation of these devices. Heat pipes, in particular, have very limited pumping capability. CPLs and LHPs have relatively high pumping capability. However, they have other difficulties such as unwarranted immediate start-up and recovery from dryout. These devices generally require a 30 W to 50 W starter heater to enhance the chances of start-up success. Numerous pumping mechanisms have been proposed as alternative pumping mechanism to assist/replace the capillary pumping. Electrohydrodynamic (EHD) pumping is a promising candidate, especially in space environment where the engineering advantages such as simple design, non-mechanical, low acoustic noise, lightweight, rapid control of performance and low power consumption are most important. Furthermore, EHD pumps provide immediate start-up operation, prompt recovery from dryout, and feasibility of micro-scale application.

The EHD phenomena involve the interaction of electric fields and flow fields in a dielectric fluid medium. This interaction between electric fields and flow fields can induce the flow motion by electric body force. The electric body force density, $\vec{f}_e$, acting on the molecules can be expressed as follows [1]

$$\vec{f}_e = q\vec{E} - \frac{1}{2}\vec{E}^2\nabla\varepsilon + \frac{1}{2}\nabla\left[\vec{E}^2\left(\frac{\partial\varepsilon}{\partial\rho}\right)_T\rho\right] \qquad (1)$$

where q is the charge density, $\vec{E}$ is the electric field, ε is the fluid permittivity, ρ is the fluid density and T is the fluid temperature. The first term represents the Coulomb force, which is the force acting on the free charges in an electric field. The second and third terms represent the polarization force acting on polarized charges. The second term, the so-called dielectric force, is related to the electric permittivity gradient. The third term, the electrostriction term, is relevant only for compressible fluids. Thus, EHD pumps require either a free space charge or a gradient in permittivity within the fluid. In an isothermal single phase liquid, $\nabla\varepsilon$ vanishes, resulting in

Coulomb force as the only mechanism for generating a permanent EHD motion.

There are two main mechanisms for generating a space charge in an isothermal liquid. The first one is associated with the ion injection at a metal/liquid interface and the related pumping is referred to as ion-drag pumping. However, the ion-drag pumping is not desirable because it can deteriorate the electrical properties of the working fluid due to ion-injection and it can be hazardous to operate. The second mechanism for generating a space charge in an isothermal liquid is associated with the process of dissociation of the neutral electrolytic species and recombination of the generated ions [2]. Under low electric field regime, dissociation and recombination are in dynamic equilibrium,

$$A^+B^- \leftrightarrow A^+ + B^- \qquad (2)$$

When an electric field exceeding a certain value (approximately 1 kV/cm, depending on the liquid characteristics) is applied, the rate of dissociation exceeds that of the recombination and it further increases at higher electric fields. Thus, there is a non-equilibrium layer where the dissociation-recombination reactions are not in equilibrium [3]. The charges generated by dissociation are redistributed in the region by the applied electric field resulting in the heterocharge layers. Heterocharge means that the charge has the opposite polarity from that of the adjacent electrode. The thickness of the heterocharge layer is proportional to the corresponding relaxation time (defined as the ratio of electrical permittivity and conductivity, and represents the time during which a charged particle maintains its charge in a medium) of the working fluid, τ, and the strength of the local electric field. The attraction between the electrode and the charges within the heterocharge layer induces a fluid motion near the electrode from the liquid side to the electrode side. This type of pumping is referred to as the conduction pumping. Considering an electrode configuration as shown in Fig. 1, the strong electric fields build up the heterocharge layers around the electrodes. With this electrode configuration, the net axial motion around the ring ground electrode is almost canceled because of the geometrical symmetry. Thus, the motion around the high voltage electrode primarily contributes to the net axial flow.

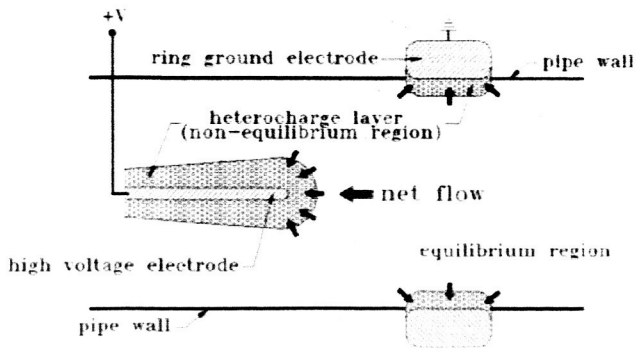

Figure 1 Illustration of EHD conduction pumping mechanism

Since the electric field is high near the high voltage electrode, the thickness of the corresponding heterocharge layer and the pressure across it will be high as well. Therefore, the flow direction will be from the ground electrode to the high voltage electrode. The current versus voltage behavior in this regime is sub-ohmic showing only a slightly increased current with increased voltage. The details of the EHD conduction pumping mechanism can be found in Atten and Seyed-Yagoobi [2], Jeong and Seyed-Yagoobi [4] and Jeong et al [5].

This paper investigates the performance of an EHD conduction pump to evaluate its feasibility for the thermal control in a two-phase loop with high heat flux source. Specifically, an EHD conduction pump, consisting of six electrode pairs, was built and installed in the two-phase loop with condenser and high heat flux evaporator (HE). The test matrix varied the applied voltage of EHD pump, the sink temperature and the heat load on the evaporator. The pressure head generated with this EHD pump, the current, the mass flow rate, and pressure drop across the HE were measured varying the applied voltage, the heat load and the sink temperature. The critical heat flux is determined at 5, 10, 15 kV and the recovery from dryout condition is demonstrated. The influence of the fluid temperature and pressure oscillation by boiling process in HE on the EHD pump performance is also investigated. The working fluid used is degassed R-134a.

NOMENCLATURE

$\vec{E}$ = electric field
$\vec{f}_e$ = electric body force density
q = net electric charge density
T = Temperature
V = voltage
ε = electric permittivity
ρ = fluid density
σ = electric conductivity
τ = charge relaxation time ($=\varepsilon/\sigma$)

EXPERIMENTAL APPARATUS

EHD conduction pump

The EHD conduction pump consists of six electrode pairs. The high voltage electrodes are fabricated from one large-radius of tube and six small-radius of tubes while the ground electrodes are made as rings, flushed against the pump inner wall. The high voltage and ground electrodes are made of stainless steel. Figure 2 presents the cross section of the high voltage electrode of the EHD conduction pump. The edges of high voltage electrode were coated with gold to remove/reduce any sharp edges. In EHD conduction pump, the electrode with less sharp points or edges is required to reduce the concurrent effects of ion injection which act against the conduction pumping. Figure 3 shows the assembled EHD conduction pump. The open area of the high voltage electrode is 58.3 % of

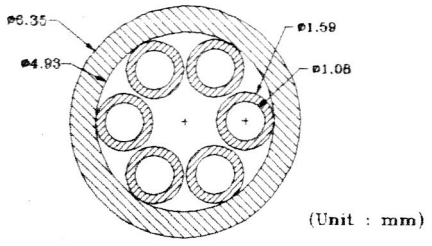

Figure 2 Crosssection of the high voltage electrode of EHD conduction pump

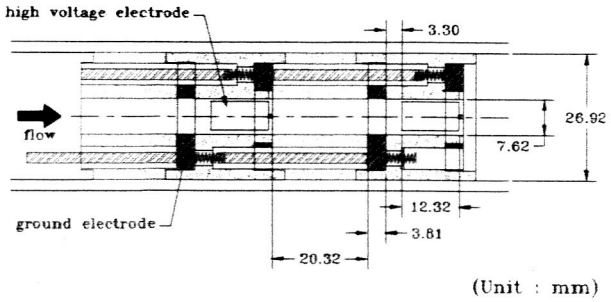

Figure 3 Assembled high voltage electrode and ground electrode (two pairs shown)

the pumping section implying that 41.7 % of the pumping section is the projected area available for heterocharges. From the EHD conduction pumping point of view, the electrode which has higher available projected area (perpendicular to axial direction) for heterocharges induces stronger net flow motion from the ground electrode toward the high voltage electrode. However, at the same time, the enough percentage of the opening area and small pressure drop across the electrode should be secured in order to provide required mass flow rate.

Two-phase loop

Figure 4 illustrates the experimental setup of the two-phase loop with EHD conduction pump. The loop consists of EHD conduction pump, condenser, preheater, high heat flux evaporator (HE), reservoir and transport lines. The total length of the loop is approximately 10 m. The inner diameter of the transport lines is 8.1 mm. The EHD conduction pump was installed on the liquid passage after the condenser. Two heaters (preheater and HE) were installed after the EHD pump section. The HE was incorporated in the loop to simulate high heat flux source in a laser application. The reservoir is located between the condenser and EHD pump. A heater controlled the reservoir temperature that determined the saturation temperature of the loop. The reservoir temperature was set to 28 $^{\circ}$ C for the entire test. To minimize the heat loss to surroundings, the entire experimental apparatus was wrapped with insulation materials. Heat loads were supplied to the HE through the cartridge heaters inserted to the copper block surrounding the pipe. The total heat load capacity of the HE was 700 W (two 300 W heaters and two 50 W heaters). T-type thermocouples (TC) located on the pipe surface inside the copper block (3 for upper and 3 for lower surface) as shown in Fig. 5 measured the temperatures along the evaporator surface. These thermocouples are positioned at 19.05 mm intervals. The heat was removed at the condenser that was connected to a recirculating chiller. The temperatures of condenser were measured by T-type thermocouples located along the condenser length. The temperatures at inlet and outlet of the condenser were also measured by thermocouples. The flow-rate of the re-circulating refrigerant through the loop was

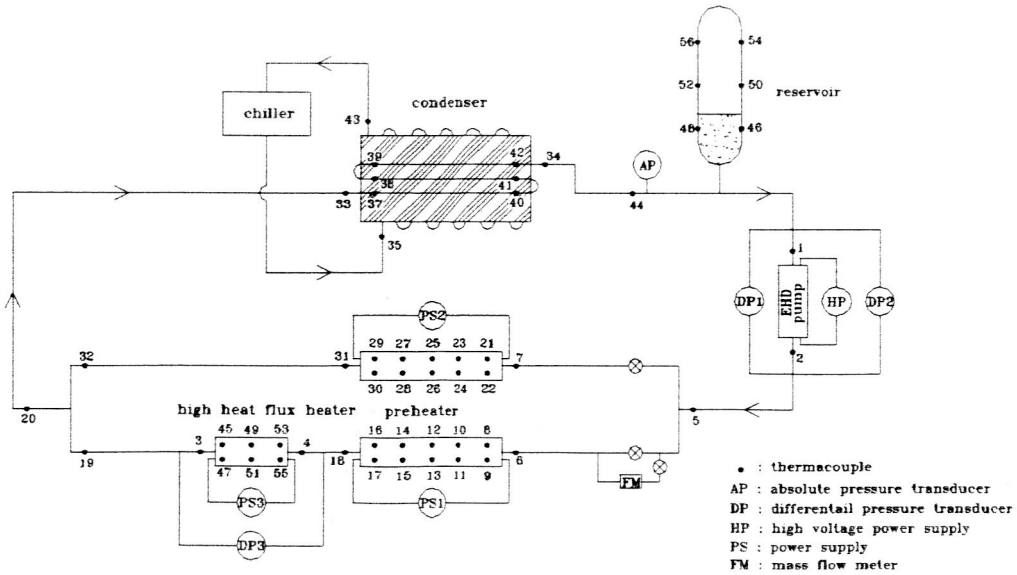

Figure 4 Experimental setup of the test loop with EHD conduction pump

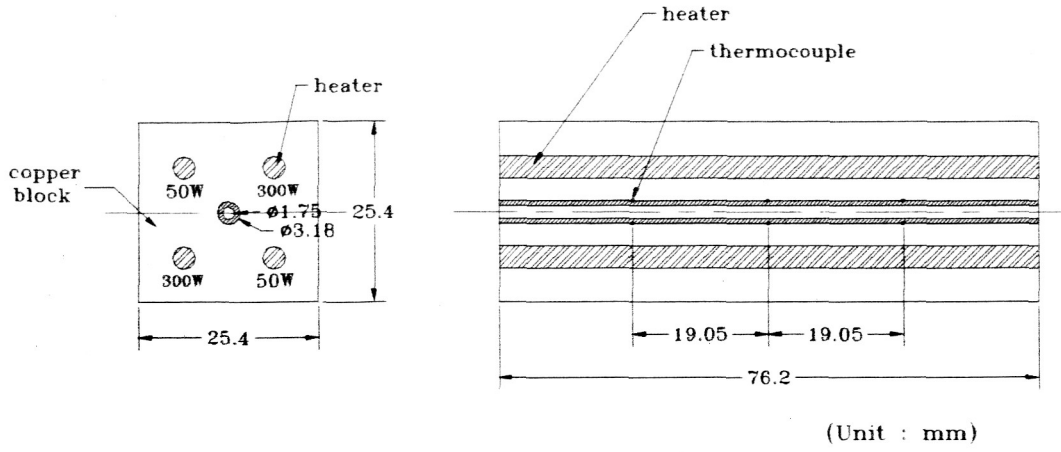

Figure 5 High heat flux evaporator

measured using a flowmeter (Model : DS006S) from Micron Motion, Inc., installed before the preheater section. The absolute pressure was measured at a location between the condenser and the reservoir via pressure transducers. The differential pressures through the EHD conduction pump and the HE were also measured using the differential pressure transducer. The differential pressure transducer through the HE is dedicated for the measurement of boiling effect on the pressure drop.

RESULTS AND DISCUSSIONS

Figure 6 (a) and (b) present the time line of the generated pressure and current, respectively, as the applied voltage varies at ambient temperature without operating the heater and condenser. This test was carried out in order to investigate the basic performance of the EHD pump in a single phase. T1 and T2 represent the EHD pump inlet and outlet temperature, respectively. The generated pressure is maintained over with time while the current decreases with time at a given applied voltage. This implies that the electric power consumption decreases with time. The maximum pressure head achieved with six pairs is approximately 9700 Pa at 16.0 kV with 3.33 W maximum electric power consumption. As presented in Fig. 6 (a) and (b), temperature difference across the EHD pump increases as the applied voltage increases. The maximum temperature difference across the EHD pump is approximately 1 °C at 16 kV. The temperature increase across the EHD pump seems to be resulted from Joule heating which can be expressed as $J = \sigma E^2$ where σ is the electric conductivity of the working fluid and E is the electric field. The Joule heating resulting from the applied electric field is usually negligible relative to the transported heat by EHD pumping since the electric conductivity of the working fluid is very low.

To investigate the long-term performance of the EHD pump, the generated pressure was measured over 46 hours. Figure 7 presents the generated pressure and the pump inlet and outlet temperature with time at 10 kV of applied voltage. The generated pressure was maintained at a level in daily mean value even though it oscillated with a period of 24 hours within 300 Pa. It is clear that the generated pressure oscillation depends on the pump inlet and outlet temperature oscillations resulting from ambient temperature variations. In order to investigate the temperature influence on the EHD conduction pump performance, the chiller set point temperature was varied from 20 °C to –20 °C at a given voltage. Figure 8 shows the variation of the generated pressure and EHD pump inlet and outlet temperature as the chiller set point changes at 10 kV of applied voltage. The generated pressure increases as the temperature of the working fluid decreases. Figure 9 presents the generated pressure at 10 kV and 15 kV and the electrical permittivity of R134a as a function of the average temperature within the EHD pump. The electrical permittivity of R134a was obtained from Bryan [6]. Note that the generated pressure is closely associated with the electrical permittivity which is function of the temperature. This is consistent with the fact that the resultant force for conduction pumping in the needle-plate configuration, analytically estimated by Atten and Seyed-Yagoobi [2], can be expressed as

$$F = -\frac{3\pi}{8}\frac{\varepsilon V^2}{\left[\ln(R/r_o)\right]^2}, \qquad (3)$$

where V is the applied voltage. In the above equation, r_o and R are the radius of the high voltage electrode and the pumping section, respectively. In conduction pumping mechanism point of view, the generated pressure increase with temperature decrease can be explained in terms of relaxation time. Considering the electric conductivity in Ohmic region, the relaxation time is 2.38 ms and 4.04 ms at 20 °C and –5 °C, respectively. The increased relaxation time at lower temperature induces thicker heterocharge layers, creating more pressure generation. The electric permittivity and electric

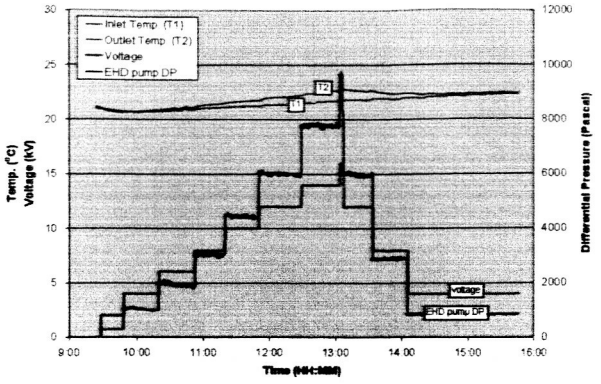

(a)

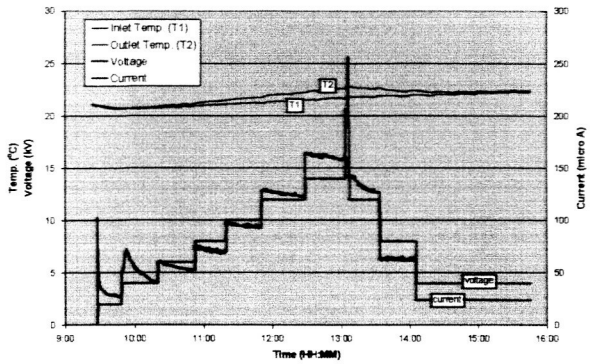

(b)

Figure 6 (a) timeline of the generated pressure, (b) timeline of the current, as the applied voltage varies (2/4/6/8/10/12/ 14/16/8/4 kV)

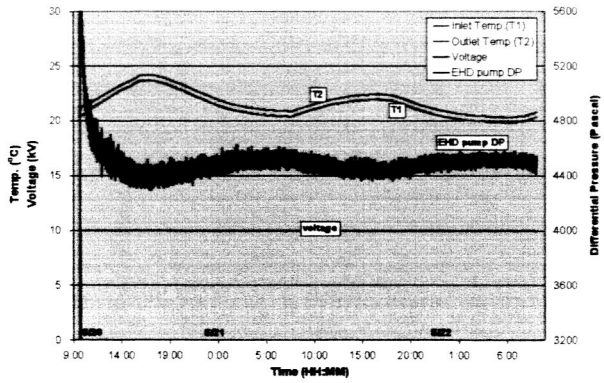

Figure 7 Generated pressure and inlet and outlet temperature of EHD pump at 10 kV of the applied voltage

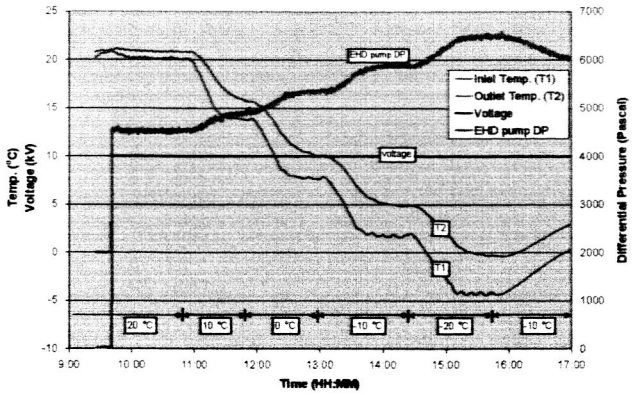

Figure 8 Generated pressure and inlet and outlet temperature of EHD pump at 10 kV of the applied voltage as the sink temperature varies (20/10/0/-10/-20/-10 °C)

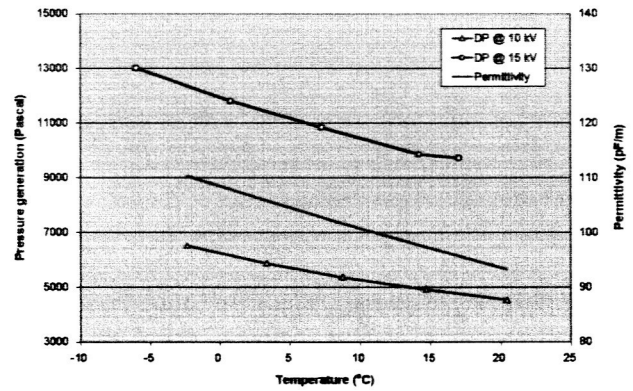

Figure 9 Generated pressure and permittivity as a function of temperature

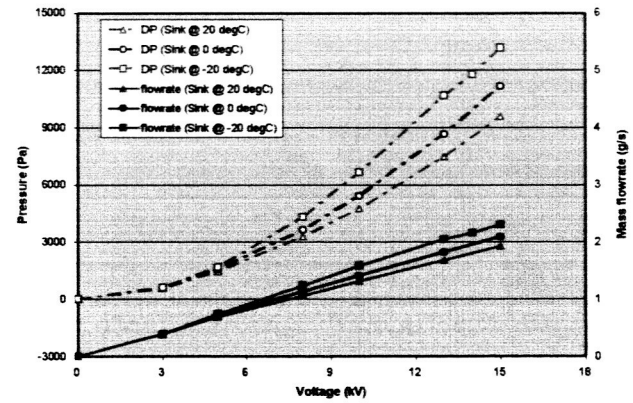

Figure 10 Generated pressure and mass flowrate as a function of the applied voltage

conductivity used for the calculation of the relaxation time were obtained from Bryan [6]. Figure 10 presents the pressure generation and mass flowrate as a function of the applied voltage for the sink temperatures of 20 °C, 0 °C, -20 °C. The pressure generation and the mass flowrate at 15 kV of the applied voltage are approximately 9570 Pa, 11170 Pa, 13160 Pa and 1.92 g/s, 2.10 g/s, 2.31 g/s at 20 °C, 0 °C, -20 °C of sink temperature, respectively.

As presented in Fig. 10, the pressure generation has quadratic dependence on the applied voltage while the mass flowrate has linear dependence on the applied voltage. This implies that the total pressure loss is proportional to the 2nd power of the velocity. Note that the quadratic dependence of the pressure generation on the applied voltage is also consistent with $F = -\frac{3\pi}{8}\frac{\varepsilon V^2}{[\ln(R/r_0)]^2}$ by Atten and Seyed-Yagoobi [2].

Figure 11 presents the timeline of the generated pressure of EHD pump, the pressure drop across the HE, the maximum temperature, and the heat load on the HE at 10 kV of the applied voltage on EHD pump and 0 °C of sink. The maximum temperature usually locates at the end of HE (TC45). The maximum temperature increased to 30 °C after applying 10 W of heat load, however the boiling did not occur at this point even if the surface temperature surpassed the saturation temperature, 28 °C, set by reservoir temperature. The boiling occurred at 15 W of heat load when maximum temperature reached 35.3 °C, and the temperature dropped rapidly because of the enhanced heat transfer by the boiling process. Therefore, the wall superheat required for the onset of boiling is approximately 7.3 °C for this condition. Note that the wall superheat required for the onset of boiling depends on surface and fluid properties. The generated pressure of EHD pump decreases with time due to temperature increase in EHD pump section caused by increasing the heat load. Dryout occurred at 95 W of heat load with this test condition.

The pressure drop across the HE and the mass flowrate as a function of heat load are presented in Fig. 12. The pressure drop increased and reached a maximum of around 3260 Pa at 65 W as the heat load increased, however it decreased beyond 65 W of heat load and reached approximately 2890 Pa at 95 W. On the other hand, the mass flow rate decreased and reached a minimum of around 0.46 g/s at 85W as the heat load increased, and then increased to 0.49 g/s during the dryout point (i.e. 95W of heat load). This inconsistency implies that pressure drop in transport line after the HE is higher at 75 W, 85 W than that of 65 W. This is probably due to the increased acceleration pressure loss in the transport line after the HE from the higher void fraction at 75 and 85 W of heat load. The pressure drop decreased and the mass flowrate increased during the dryout, implying that the vapor-phase pressure drop is lower than the two-phase pressure drop. The above-mentioned trends of the pressure drop with heat load (i.e the pressure drop increases with heat load until a certain point and decreases beyond that point), were observed in all tests with boiling phenomena. This

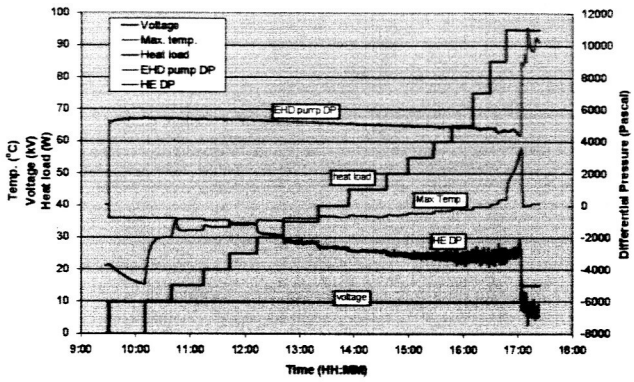

Figure 11 Timeline of the generated pressure of EHD pump, pressure drop across the HE, heat load on the HE, the applied voltage on EHD pump, and the maximum temperature at 0 °C of sink

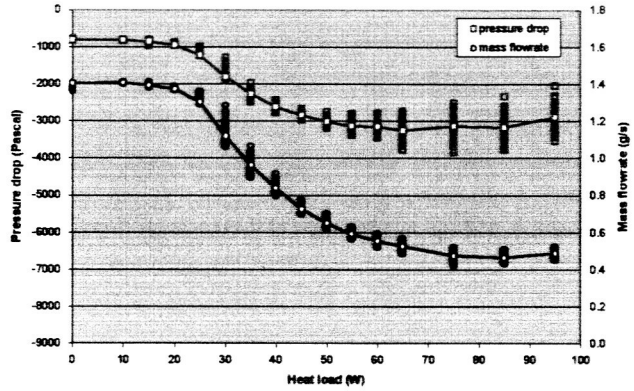

Figure 12 Generated pressure and mass flowrate as a function of heat load

implies that the two-phase pressure drop increases with void fraction increase until a certain value but reduces beyond that point. The data confirms that the two-phase pressure drop during boiling is a function of flow regime. As the vaporization process proceeds, the flow will usually encounter bubbly, plug, annular, and mist flow regime along the HE depending on the applied heat flux and the flow entrance condition. Depending on the mass flow rate, the bubbly and the plug flow regime will be dominant at low heat flux, while the annular and the mist flow regime will be dominant at high heat flux. The oscillation of the pressure drop at the HE, seems to be caused by unstable boiling process, also varies as the boiling process develops. It usually increases as the heat load increases until a certain point. It was more significant with low flow rate.

Figure 13 presents the maximum heat flux and power consumption of EHD pump as a function of the applied voltage

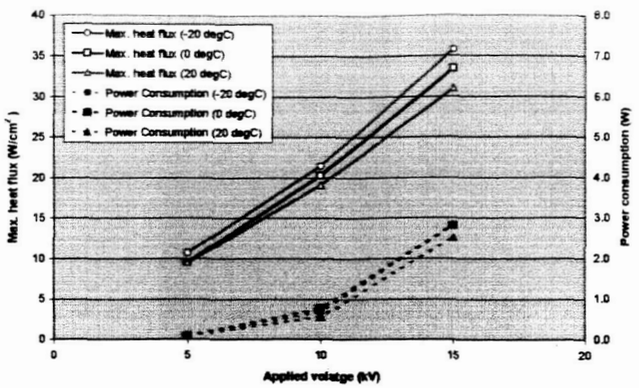

Figure 13 Critical heat flux and power consumption of EHD pump as a function of the applied voltage at −20°C, 0 °C, 20 °C of sink temperature

at 20 °C, 0 °C, -20 °C sink temperature, respectively. The power consumption in Fig. 13 corresponds to the value in approximately 8 hours operation. The power consumption decreases with time since the current usually shows the maximum value at initial operation and decreases with time approaching to a nearly constant value after long operation. The maximum heat flux increases as the sink temperature decreases. The maximum heat flux at 20 °C sink temperature for 5 kV, 10 kV, 15 kV are approximately 9.5 W/cm^2, 19.1 W/cm^2, 31.0 W/cm^2 with 0.094 W, 0.56 W, 2.52 W of EHD power consumption, respectively. The maximum heat flux at 0 °C sink temperature for 5 kV, 10 kV, 15 kV are approximately 9.5 W/cm^2, 20.3 W/cm^2, 33.4 W/cm^2 with 0.095 W, 0.77 W, 2.82 W of EHD power consumption, respectively. The maximum heat flux at –20 °C sink temperature for 5 kV, 10 kV, 15 kV are approximately 10.7 W/cm^2, 21.5 W/cm^2, 35.8 W/cm^2 with 0.094 W, 0.68 W, 2.84 W of EHD power consumption, respectively. The superheat required for the boiling onset was ranged between 5.0 °C and 12.4 °C. It did not show any specific dependency on parameters such as mass flowrate, heat loads, sink temperature, and HE inlet temperature. The maximum heat load at 15 kV was 150 W with –20 °C of sink temperature, providing approximately 1500 W·m of heat transport capacity. The maximum power consumption percentage over the heat load transported is 1.94 %, 2.02 %, and 1.89 % at 15 kV for 20 °C, 0 °C, -20 °C of sink temperature, respectively. Note that the pump pressure generation and the heat transport capacity could be increased simply by increasing the number of the electrode pairs at the same applied voltage.

In order to confirm the temperature control and demonstrate the recovery from dryout condition, the test was carried out in the following procedures. Initially, the chiller was turned on with a set point temperature between –20 °C and 20 °C and 5 kV was applied to EHD pump. Once the chiller reached the steady state, the electric power to heaters was turned on. The power to heaters was maintained constant until the test parameters such as the temperatures at HE, pressure generation through EHD pump and mass flowrate reached steady state, and stepped up by 20 W to a higher level. The increase of the heat load to the HE continued until the dryout occurred in the HE or the temperature reached a pre-determined maximum temperature, 60 °C. The applied voltage on the EHD pump was then stepped up by 5 kV after the dryout proceeded for a period of time. Once the dryout was recovered and the temperature of the HE reached a steady state, the heater power was again increased to a higher level. The increase in heat load to the HE continued until the dryout of the evaporator started again. Figure 14 presents the timeline of the measured pressure generation across EHD conduction pump and the pressure drop across the HE and the maximum temperature in the loop when the heat load on HE was varied from 20 W to 100 W by 20 W at 0 °C chiller set temperature. The negative sign in pressure indicates the pressure drop and the positive sign indicates the pressure generation by EHD pump. 5.14W of heat load was applied to preheater before applying the heat load on the HE. The voltage on EHD pump was initially applied with 5 kV and increased by 5kV when dryout occurred. When 25.14 W of heater load including preheater load was applied, boiling initiated and pressure drop across the heater increased approximately from 168 Pa to 819 Pa. The maximum temperature peaked at 36.5 °C before boiling started and dropped to 31.7 °C because of the enhanced heat transfer by the boiling. The maximum temperature reached 60 °C at 45.14 W of heater load but dropped rapidly to 35 °C when the applied voltage on EHD pump increased to 10 kV. At 10 kV, the HE load increased by 20 W to 100 W and the maximum temperature started to increase to the limit at 100 W of the HE load. The maximum temperature dropped rapidly to 41 °C by increasing the applied voltage to 15 kV. The pressure drop across the heater increased approximately from 2550 Pa to 6470 Pa mainly because of the increased mass flow rate at 15 kV of the applied voltage. The same test procedure was applied for –10 °C chiller set temperature and the results are presented on Fig. 15. The boiling occurred at 25.14 W of total heat load when the maximum temperature reached to 40.6 °C. Note that the wall superheat required onset of boiling is 12.6 °C with -10 °C of sink while that is 8.5 °C with 0 °C of sink. Similarly, the dryout occurred at 45.14 W and 105.14 W of the total heat load for 5 kV and 10 kV of the applied voltage, respectively. The maximum temperature increased during dryout at 5 kV and 10 kV dropped rapidly when the applied voltage increased to 10 kV and 15 kV, respectively.

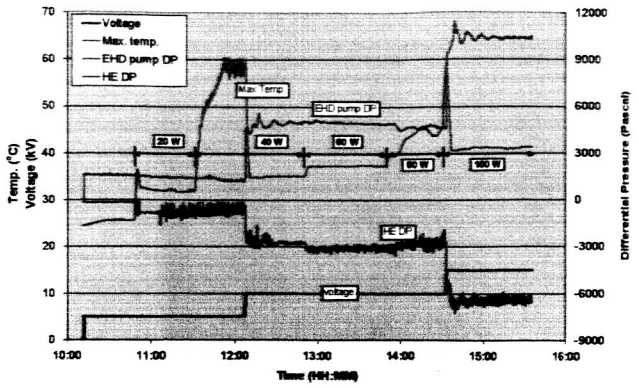

Figure 14 Timeline of the generated pressure of EHD pump, pressure drop across the HE, the applied voltage on EHD pump, and the maximum temperature at 0 °C of sink

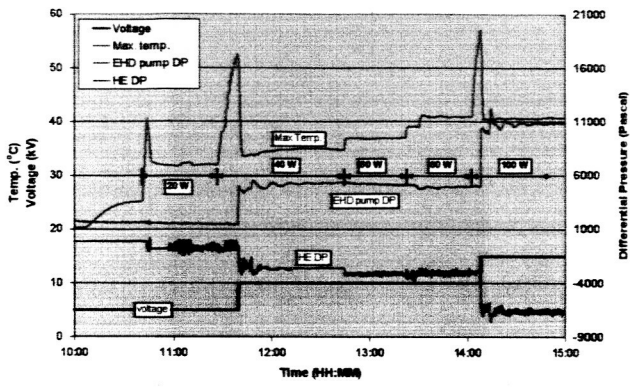

Figure 15 Timeline of the generated pressure of EHD pump, pressure drop across the HE, the applied voltage on EHD pump, and the maximum temperature at -10 °C of sink

It was observed in the entire test with heater operation that the pressure drop oscillation across the HE exists during boiling. The pressure drop oscillation varied as the boiling process developed and presented even higher than 2000 Pa in magnitude, however, the EHD pump operated consistently without a significant perturbation or performance deterioration. This seems to be because the oscillation is damped out through the long transport lines and the condenser capacity is enough so the EHD pump always operates in single liquid phase.

CONCLUSION

An EHD conduction pump which utilizes the heterocharge layers in the vicinity of the electrodes was built and installed in the liquid passage of a two-phase loop to investigate the heat transport capacity (maximum heat flux) and confirm the satisfactory operation in the two-phase loop. The EHD conduction pump presented the satisfactory operation even when the loop has two-phase fluid and a significant pressure oscillation by boiling occurred in the HE section. Furthermore, the EHD conduction pump provided immediate recovery from dryout condition by simply increasing the applied voltage. The EHD conduction pump operated at 15 kV presented pressure head on the order of 13000 Pa with less than 2.84 W of electric power at -20 °C of sink temperature providing thermal control capacity for 35.8 W/cm^2 of heat flux and 1500 W·m of heat transport with R134a as the working fluid. Note that the thermal control capacity can be increased by enhancing the evaporator surface and/or simply increasing the number of the electrode pairs. It was also confirmed that the performance of EHD conduction pump depends on the operating temperature. The performance evaluation over long period of time (months or years) needs to be carried out in order to investigate the reliability and steadiness of the EHD pump.

ACKNOWLEDGMENT

This work was supported by National Research Council and NASA Goddard Space Flight Center Laser Risk Reduction Project.

REFERENCES

1. Melcher, J. R., 1981, *Continuum Electromechanics*, Cambridge, MIT Press.

2. Atten, P. and Seyed-Yagoobi, J., 2003, "Electrohydrodynamically Induced Dielectric Liquid Flow Through Pure Conduction in Point/Plane Geometry", *IEEE Transactions on Dielectrics and Electrical Insulation*, Vo. 10, No. 1, pp 27-36.

3. Zhakin, A. I., 1998, "Conduction Models in Dielectric Liquids", *Electrohydrodynamics*, edited by A. Castellanos, Chapter 6, Springer Wien New York.

4. Jeong, S.I. and Seyed-Yagoobi, J., 2002, "Experimental Study of Electrohydrodynamic Pumping Through Conduction Phenomenon", *Journal of Electrostatics*, Vol. 56, pp. 123-133.

5. Jeong, S.I., Seyed-Yagoobi, J., and Atten, P., 2003, "Theoretical/Numerical Study of Electrohydrodynamic Pumping Through Conduction Phenomenon", *IEEE Transaction on Industry Application*, Vol. 39, No. 2, pp. 355-361.

6. Bryan, J.E., 1998, *Fundamental Study of Electrohydrodynamically Enhanced Convective and Nucleate Boiling Heat Transfer*, Ph. D. Dissertation, Department of Mechanical Engineering, Texas A&M University, College Station, Texas.